J Radioanal Nucl Chem
DOI 10.1007/s10967-016-4924-0

Interaction mechanisms of U(VI) and graphene oxide from the perspective of particle size distribution

Yanan Wang[1,2] · Xia Liu[1,2] · Yongshun Huang[1,2] · Tasawar Hayat[3] · Ahmed Alsaedi[3] · Jiaxing Li[1,3]

Received: 26 April 2016

Abstract Graphene oxide (GO) is an ideal adsorbent due to excellent physicochemical properties. Humic acid (HA) is ubiquitous in aquatic and soil environment, which can affect the migration of metal ions. In this study, we investigated the sorption mechanisms of U(VI) onto GO surfaces in the presence of HA. pH dependent and ionic strength independent sorption process were observed and the concentration of HA is positively proportional to U(VI) sorption capacities. Results also suggest that a pre-mixing HA + U(VI) gave better results than a pre-mixing of GO + HA, which can be explained by the size distribution of different GO systems.

Keywords Graphene oxide · U(VI) sorption · Humic acid · Size distribution

Introduction

Uranium(VI) is a typical radioactive element for nuclear power plants because of its high fission energy [1] and the fast development of U(VI) industry made uranium a common contaminant to soils, surface and groundwater [2, 3]. Various technologies such as filtration, surface complexation, chemical precipitation, ion exchange, sorption, electrodeposition, and membrane processing are applied to remediation of uranium ions from aqueous solution [4–6]. Sorption technique is widely adopted due to its convenient operation, cost-efficiency and environmental friendliness [7]. GO has emerged as a new sorbent with excellent properties because of its abundant oxygen-containing functional groups, including hydroxyl, carboxylate, and epoxide.

Investigations about the sorption of metal ions to GO are abundant. For example, as reported by Yang et al. [8], the maximum sorption capacities of GO toward Pb(II), Ni(II), and Sr(II) were determined to be 2.37, 1.75, and 0.62 mmol g^{-1}, respectively and Pb can easily abstract the OH group from the GOs to form the much more stable Pb(OH)–GO complex. Gopalakrishnan et al. [9] reported that GOs could remove heavy metal ions effectively with the permissible pH of 8.00 from pharma–effluent with low adsorbent dosage of GO nanosheets. Wang et al. [10] also investigated the adsorption of U(VI), $^{152+154}$Eu(III), $^{85+89}$Sr(II) and ^{134}Cs(I) onto GO, indicating that GOs had much higher sorption capacities than many other contemporary materials for the preconcentration of radionuclides. The examples and data above can lead to the conclusion that GO has excellent sorption performance toward heavy metal ions. In general, the sorption of metal ions can change the particle size of GO. For instance, Sitko et al. [11] investigated the dispersibility of GO in water and found that it changes remarkably after complexation of Cu^{2+}, Zn^{2+}, Cd^{2+} and Pb^{2+}. Romanchuk et al. [12] reported similar phenomenon as well and the critical coagulation concentration of GO with different cations (Na^{+}, Ca^{2+} and Eu^{3+}) varies at pH 3 and 7. What's more, Eu(III) and U(VI) facilitated GO

Electronic supplementary material The online version of this article (doi:10.1007/s10967-016-4924-0) contains supplementary material, which is available to authorized users.

✉ Jiaxing Li
lijx@ipp.ac.cn

[1] Institute of Plasma Physics, Chinese Academy of Sciences, P.O. Box 1126, Hefei 230031, People's Republic of China

[2] University of Science and Technology of China, Hefei 230026, People's Republic of China

[3] NAAM Research Group, Faculty of Science, King Abdulaziz University, Jeddah 21589, Saudi Arabia

Published online: 05 July 2016

aggregation was observed with high Eu(III) and U(VI) concentration and may be caused by surface charge neutralization of GO after sorption, as reported by Xie et al. [13]. The change of GO particle size distribution after adsorption can pose a significant difference in the mobility and separation of GO–metal ions afterward. The phenomenon was reported by Liu et al. [14] that the velocity of GO nanosheets was inversely proportional to its radius and the closer to the anode of the samples, the smaller the average lateral-dimensional sizes and vice versa. Thus, studying the distribution of GO particle size after U(VI) sorption is of great significance.

Humic acid (HA), a natural organic polymer, is widely spread in soil organic substances, peat, lignite, weathering coal and sediments of lakes and oceans [15, 16]. It contains versatile functional groups such as carboxylic, phenolic, carbonyl, and hydroxyl groups that connected with either aliphatic or aromatic carbons in the macromolecules [17]. Therefore, it will affect the removal and mobility of metal ions by various materials and thereby potentially alter the fate and transportation of heavy metals in aquatic environment [18]. Besides, HA has both hydrophilic and hydrophobic moieties [19], making it be able to change the surface properties, and toxicity of nanomaterials, and more importantly, HA can affect the size distribution of nanomaterials [20, 21].

In this paper, we investigated the factors that might have an influence on the particle size distribution of GO nanosheets through sorption experiments, especially the solution pH, metal ions concentration, HA and even the mixing orders of ingredients. Based on that, sorption behaviors of U(VI) by GOs under various conditions were studied and the interaction mechanisms of GOs and U(VI) was given particularly from the perspective of particle size distribution as well.

Experimental section

Materials

The UO_2^{2+} stock solution (1.0 mmol L^{-1}) was prepared from its nitrate (99.9 %, Sigma-Aldrich) after dissolution and dilution with 0.01 mol L^{-1} HNO_3 solution. All chemicals were purchased in analytical-reagent grade and used in the experiments directly without any further purification. Deionized water was used for the GO preparation and adsorption studies.

Synthesis of GOs

Modified Hummers method [22] was used to produce GOs from graphite. Specifically, under vigorous stirring, a mixture of graphite (1.5 g), $NaNO_3$ (1.5 g) and H_2SO_4 (60 mL) were placed in an Erlenmeyer flask and cooled with an ice bath. $KMnO_4$ (9.0 g) was slowly added into this solution. The remaining mixture was stirred at 20 ± 1 °C for 5 days, followed by adding deionized water (120 mL). This solution was then agitated at 90 °C for 40 min before cooled to 60 °C. The excess $KMnO_4$ was removed by slowly adding H_2O_2 (30 %, 6 mL). The solid residue was filtered, washed with deionized water and dried under vacuum to obtain the desired GOs, which was dispersed into water by vigorous stirring and ultrasonication if necessary, to make stock solutions.

Characterizations

The morphologies and microstructures of GO were characterized by scanning electron microscopy (SEM, FEI Sirion-200) and transmission electron microscope (TEM, JEOL JEM-2010, 200 kV). Fourier transform infrared spectroscopy (FTIR) were conducted on Nicolet Magana-IR 750 spectrometer. The zeta-potential of GO and HA as well as particle size of different systems were conducted on a ZETASIZER 3000 HSA system.

Sorption experiments

All batch sorption experiments were carried out in polyethylene tubes. Stock solution of U(VI) (1.0 mM L^{-1}) was prepared and diluted to desired concentrations if necessary. The solution pH was adjusted using negligible amounts of NaOH and/or HCl solutions. To determine the adsorption kinetics, experiments were carried out in a 200 mL conical flask. At desired time intervals, 6 mL volumes of suspension were pipetted from the conical flask and samples were centrifuged at 8000 r min^{-1} for 20 min. The solution concentration (supernatant level) was measured by spectrophotometer at the wavelength of 669 nm, using chlorophosphonazo III as the color agent. At a constant adsorbent concentration (0.133 g L^{-1}), the adsorption isotherms of U(VI) were obtained by carrying out the adsorption experiments with different initial concentrations of U(VI). The thermodynamic data was calculated by performing adsorption experiments at temperatures of 298, 308, and 318 K.

The sorption percentage (%), distribution coefficient (K_d) and amount of adsorbate adsorbed on GO (Q_e) were calculated by the following equations:

$$\text{Sorption } (\%) = \frac{C_0 - C_e}{C_0} \times 100 \quad (1)$$

$$K_d = \frac{C_0 - C_e}{C_0} \times \frac{V}{m} \quad (2)$$

$$Q_e = \frac{(C_0 - C_e) \times V}{m} \quad (3)$$

where C_0 (mg L^{-1}) and C_e (mg L^{-1}) are the initial and equilibrium concentrations of U(VI) in the solution, V (L) is the total volume of the suspension, and m (g) is the mass of adsorbent. Influencing factors, including the contact time, pH, ionic strength and temperature were also investigated. All the experimental data were the average of duplicate determinations and the relative errors were within 5 %.

Results and discussion

Characterization of GO

The surface morphologies of GO were examined by SEM and TEM, as shown in Fig. 1. SEM image (Fig. 1a) indicated randomly aggregated, thin and crumpled sheets of GO [23, 24]. The size of GO can be observed by TEM image (Fig. 1b), being 0.3–2.0 μm in width and about 1 nm in thickness.

The surface charges of GO and HA was measured by potentiometric acid–base titrations (Fig. 2), indicating negatively charged surfaces for both GO and HA within the experimental pH ranges. A higher negatively charged surface of GO than HA was observed at all pH values, which might be attributed to the abundant negatively charged functional groups, such as hydroxide and carboxylate functional groups. Moreover, the negative charge of GO surface decreased dramatically within pH 2.5–4.0 and maintained the high negativity at pH > 5.0.

FTIR was used to detect the functional groups on GO, as shown in Fig. 3. Versatile oxygen-containing functional groups were observed, which involved the strong and broad O–H peak at 3400 cm^{-1}, the strong C=O peak at

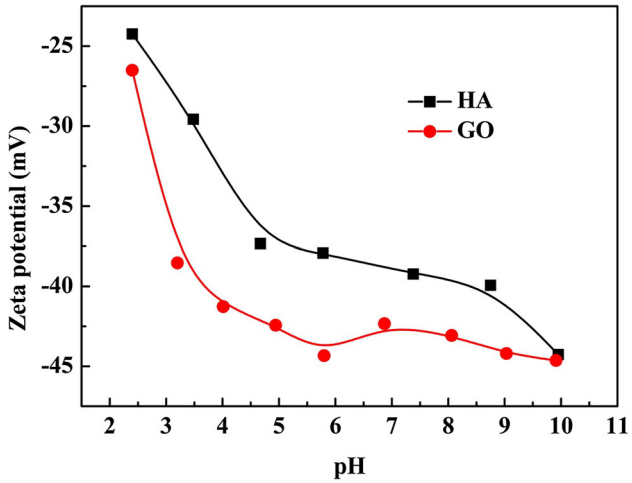

Fig. 2 Potentiometric acid–base titration of HA and GO

1740 cm^{-1}, the C–OH stretching at 1220 cm^{-1}, and the C–O stretching peak at 1050 cm^{-1}. The peaks at 1620 cm^{-1} and 1376 cm^{-1} were assigned to the vibration of adsorbed water on GO and the contribution of the skeleton C=C vibrations of graphitic domains [25]. After absorbed U(VI) in the presence of HA, the peaks at 3400, 1740, 1620 and 1376 cm^{-1} can still be observed but with different intensities, while peaks at 1220 and 1050 cm^{-1} were lost and new peaks at 1092 and 923 cm^{-1} were detected, which can be attributed to the existence of HA on the surface of GO.

The shape and size of graphene nanostructure are known to dictate its chemical properties due to the edge states and quantum confinement [26]. GO, which can be used as a precursor of graphene materials, also has unique size and/or shape-dependent properties [14]. Therefore, different synthetic techniques were applied to produce GO nanosheets with narrow sizes and shape dispersions, such as polar

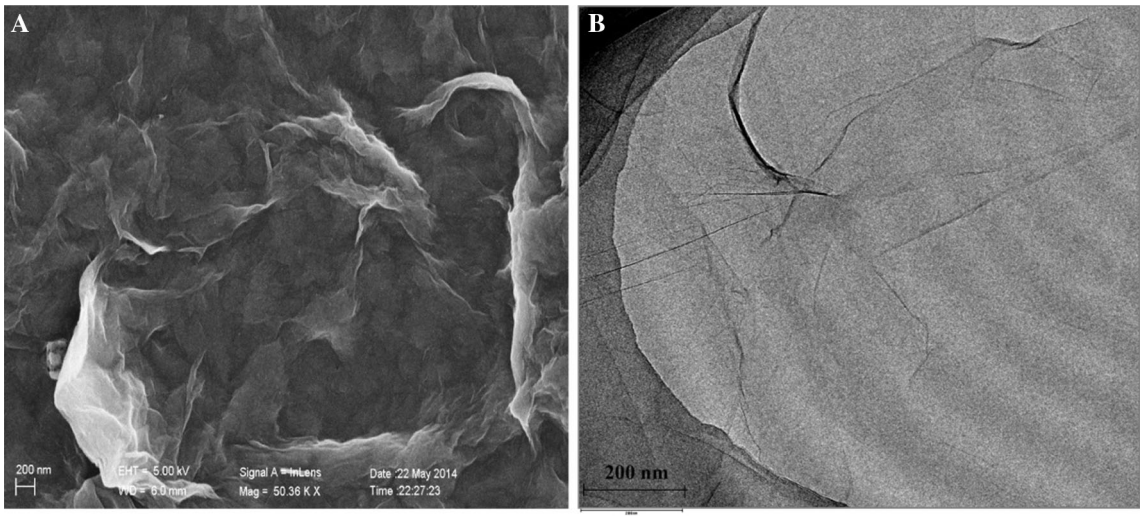

Fig. 1 SEM (**a**) and TEM (**b**) images of GO

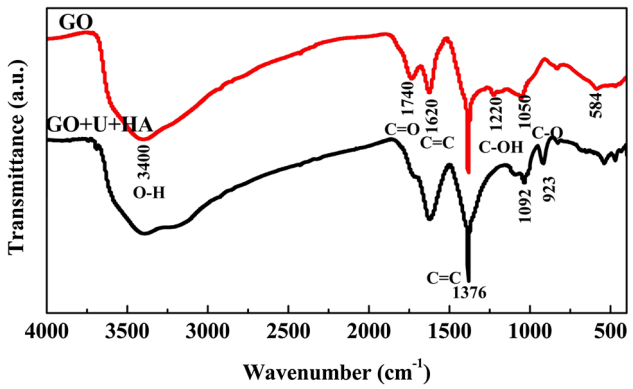

Fig. 3 FTIR spectra of GO and GO + U + HA

solvent-selective natural deposition method [27] and pH-assisted selective sedimentation [28]. The former method is based on the different dispersibility and stability of vari-sized GOs in a polar solvent while the latter one is based on the selective precipitation of GO sheets at pH 4.0, both of which were taking advantage of GO's properties in various conditions. As a matter of fact, apart from the solvent and solution pH, the size of GO nanosheets can also be affected by the existence of metal ions and humic substances [29], which are also closely dependent on the intrinsic properties of GO that can be embodied by sorption performance and parameters. As a result, sorption experiments with respect to sorption isotherms, kinetics, thermodynamics as well as reaction conditions such as ionic strength, pH and HA and so on were conducted as follows.

Sorption isotherms, kinetics and thermodynamics

The adsorption mechanism can be simulated by different sorption isotherms. While the Langmuir theory describes the quantitatively formation a monolayer adsorbate on the surface of the adsorbent, the Freundlich isotherm is usually applied to the heterogeneous surfaces. The corresponding equations are:

$$\text{Langmuir:} C_s = \frac{bC_{smax}C_e}{1 + bC_e} \tag{4}$$

$$\text{Freundlich:} C_s = K_F C_e^n \tag{5}$$

where C_e (mg L^{-1}) is the concentration of uranium after equilibrium, C_s (mg g^{-1}) is the amount of uranium adsorbed on GO, C_{smax} is the maximum of C_s and b (L mg^{-1}) is a Langmuir constant that relates to the sorption heat; K_F and n are the Freundlich constants that are in relation to sorption capacity of adsorbent and intensity of sorption, respectively. Both isothermal models were applied in the sorption of U(VI) onto GO surface, as depicted in Fig. S3 and tabulated in Table S2. Higher correlations coefficiencies were obtained for the Langmuir model, indicating a monolayer coverage adsorption mechanism.

To monitor the sorption efficiency, the sorption kinetics are often used to predict the adsorption characteristics and mechanisms. The linear form of pseudo-first, pseudo-second and intra-particle diffusion kinetic models respectively presented as:

$$\ln(Q_e - Q_t) = \ln Q_t - k_1 t \tag{6}$$

$$\frac{t}{Q_t} = \frac{1}{k_2 Q_e^2} + \frac{t}{Q_e} \tag{7}$$

$$Q_t = k_{int} t^{0.5} \tag{8}$$

The related sorption kinetic data were collected in Table S1. A higher correlation coefficient was obtained for pseudo-second order kinetic model than either pseudo-first order and intra-particle diffusion model. The sorption feasibility and spontaneity can be investigated by carrying out the sorption at different temperatures and plotting the equilibrium constant (ln K_d) versus T^{-1}, as shown in Fig. S4 and collected in Table S3. A positive enthalpy was obtained, indicating an endothermic process. However, upon counting the enthalpy change, negative free Gibbs energies were observed, resulting in a spontaneous sorption.

Effect of the presence of HA and pH on uranium sorption

The effects of HA on U(VI) sorption as a function of pH are graphically presented in Fig. 4a. The adsorption of U(VI) on GO nanosheets increased sharply within pH values of 2.5–6.0, then reached a plateau and remained constant at pH 6.0–8.0. At pH > 8, the sorption efficiency decreased. The phenomenon can be explained by the relative distribution of U(VI) species at different pH values, as simulated by PHREEQC.30 [30] in Fig. 4b. While the GO surface kept negatively charged within the experimental pH ranges (Fig. 2), the species distributions of U(VI) changed from positively charged to negatively charged with increasing pH values. Specifically, positively charged UO_2^{2+} existed as the predominant species at pH < 4.0, a mixture of hydrolyzed species of $(UO_2)_3(OH)_5^+$, $UO_2(OH)^+$ $(UO_2)_4(OH)_7^+$ and $UO_2(OH)_2$ were observed at pH 4.0–8.0. Meanwhile, negatively charged species of $UO_2(OH)_3^-$ and $(UO_2)_3(OH)_7^-$ emerged at pH 7.0 and became dominant species at pH > 9.0.

The sorption phenomenon at different pH values can be explained by the electrostatic interactions between GO and U(VI) species. At low pH values (~2.5), relatively lower negatively charged GO surface was observed due to the protonated carboxylate functional groups, which resulted in reduced hydrophilicity and increased aggregations [31] of

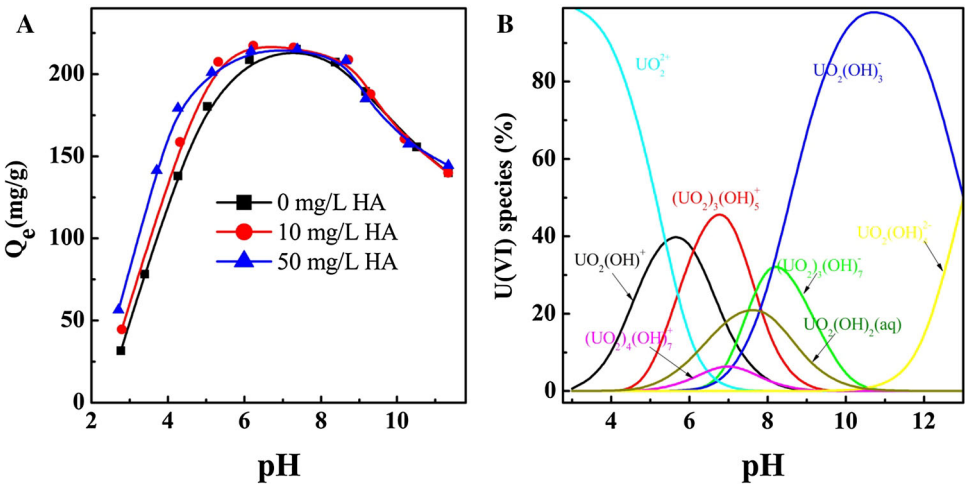

Fig. 4 **a** Effects of HA concentration and pH on U(VI) sorption; **b** effect of pH on speciation of U(VI), $C_U = 30$ mg L^{-1}, $C_{GO} = 0.133$ g L^{-1}, $T = 298$ K, $I = 0.1$ M NaCl

GO nanosheets in aqueous solution and weak sorption capacities. With increasing pH values (2.5–6.0), the GO surface was getting more and more negatively charged, which provided stronger electrostatic attraction between GO and positively charged U(VI) species. This strong interaction remained within pH 6.0–8.0. At pH > 8.0, negatively charged U(VI) species dominated, which resulted in electrostatic repulsion forces and reduced sorption capacities.

The ionic strength effect was revealed by carrying out sorption experiments in NaCl solutions (0.001, 0.01 and 0.1 M) at all pH values, as shown in Fig. S2. The weak influences suggested a dominant inner-sphere surface complexation sorption mechanism rather than an ionic exchange mechanism [32, 33], due to the fact that ionic exchange or outer-sphere surface complexation was easier to be influenced by ionic strengths than inner-sphere surface complexation [34].

The effect of HA concentrations toward U(VI) sorption onto GO was also examined and shown in Fig. 4a, which can be divided into two sections as a function of pH. While HA exhibited positive impact toward U(VI) sorption at pH 2.5–7.0, independent sorption phenomenon was observed at pH 7.0–10.0. At low pH values, GO has a tendency to aggregate due to the strong interplanar interactions and protonated carboxylate functional groups, resulting in reduced available surface areas [35, 36]. In this case, the addition of HA would promote the dispersity and stability of GO in aqueous solution [22] because of the inherent amphoteric properties of HA, which would exhibit positive effect toward U(VI) sorption by providing increased available active sites. However, when the solution turned to alkaline range, negatively charged U(VI) species $UO_2(OH)_3^-$ and $(UO_2)_3(OH)_7^-$ dominated. The electrostatic attraction was replaced by repulsion, resulted in independent sorption phenomenon.

Effect of HA concentrations on uranium sorption

The sorption capacity of GO toward U(VI) can be influenced by the presence of HA, as discussed above. Detailed sorption isotherms under three different HA concentrations (Fig. 5a) and a fitted linear relationship between the concentration of HA and the adsorbed amount of U(VI) onto GO (Fig. 5b), in which the initial U(VI) concentration was fixed, were plotted. HA can facilitate the U(VI) sorption onto GO and higher concentration of HA resulted in higher sorption capacity, as presented in Fig. 5b with a correlation coefficient of 0.9459 (linear fitting result of Excel). The addition of HA into GO solution may affect the U(VI) sorption through the following mechanisms [37]: (1) HA binds to the same active sites on GO surface as U(VI) ions, resulting in a reduced active sites for U(VI) sorption due to site blockage by HA; (2) HA interacts with GO via different sites as U(VI) does, reserving the same amount of active sites on GO surface. However, the adsorbed HA will prevent the approach of U(VI) ions to GO surface due to shielding effects [38]. In both cases, reduced sorption capacities should be obtained, which is opposite to our experimental observations. This can be explained by the abundant functional groups of HA, providing extra active sites for U(VI) binding, which will overcome the blocking and shielding effects to enhance the sorption capacity.

Effect of the orders of adding ingredients on uranium sorption

After screening the influencing factors of the presence of HA, HA concentrations, pH values and ionic strengths, the effect of sorption capacity toward the mixing orders of HA and U(VI) with GO solution was also examined, as depicted in Fig. 6. Three tests were carried out: single U(VI) sorption with fresh sorbent, simultaneous co-

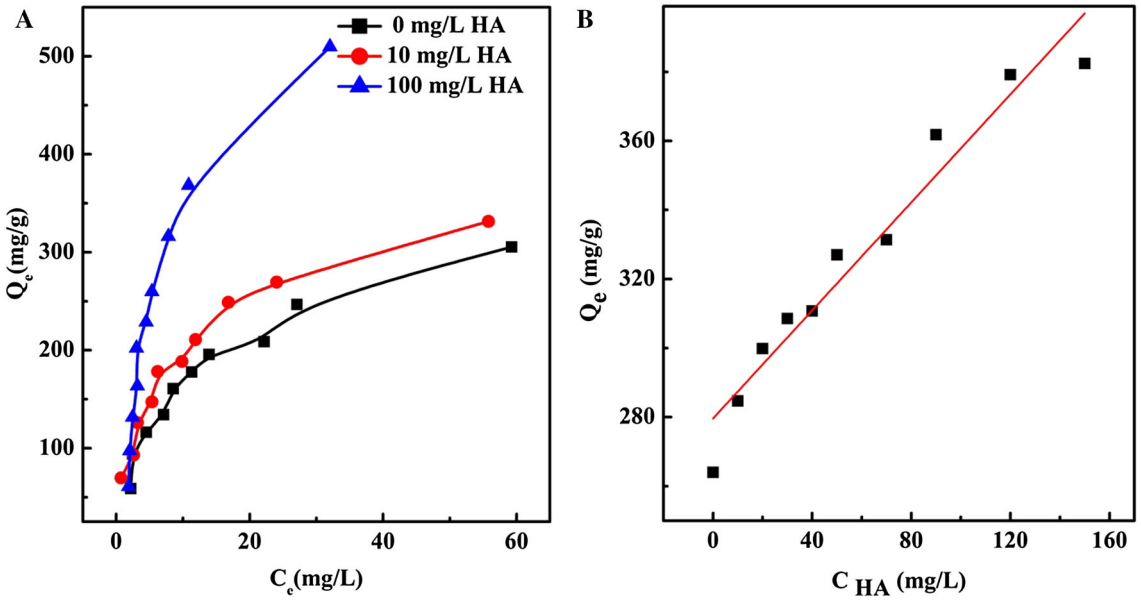

Fig. 5 **a** Sorption isotherms of uranium on GO with different HA concentration, $C_{HA} = 0$, 10, 100 mg L^{-1}, respectively; **b** plots of C_{HA} versus Q_e and corresponding linear fitting. $C_U = 60$ mg L^{-1}, $C_{GO} = 0.133$ g L^{-1}, pH = 5.0 ± 0.05, $T = 298$ K, $I = 0.1$ M NaCl

adsorption of U(VI) and HA with clean sorbent, mixing U(VI) and HA before adding GO solution (simultaneous sorption), and the addition of HA into GO solution before adding U(VI) (sequential sorption). A maximum sorption capacity was observed for the simultaneous sorption, followed by sequential sorption and single U(VI) sorption. This phenomenon is similar to the reported results for uranium sorption on CD/GO (CD: cyclodextran) [39], and can be explained as follows.

As discussed above, the presence of HA had positive influence toward U(VI) sorption onto GO, which resulted in higher sorption capacities for both simultaneous and sequential sorption than single U(VI) sorption, similar results as the copper sorption onto FRGO (few-layer reduced graphene oxide) and FGO (few-layer graphene oxide) by Yang et al. [38]. By premixing HA and U(VI), complexes would form between HA and U(VI), which would adsorb partial U(VI) ions onto HA. By adding GO solution, these complexes would further interact with GO, meanwhile, direct electrostatic interactions between free U(VI) and GO also existed, resulting in promoted sorption capacity. For sequential sorption, although extra active sites will be provided from HA by premixing HA and GO. The negative effect from blocking and shielding effects, as discussed above, will reduce the overall sorption capacities, resulting in a slightly lower sorption capacity than simultaneous sorption.

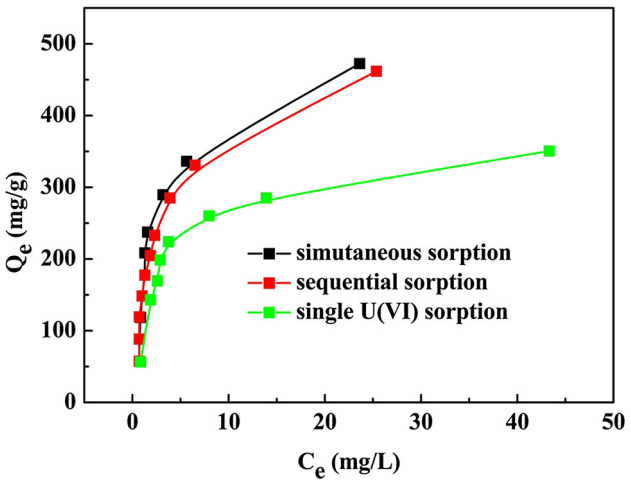

Fig. 6 Sorption isotherms of different adding orders, $C_{HA} = 100$ - mg L^{-1}, $C_U = 60$ mg L^{-1}, $C_{GO} = 0.133$ g L^{-1}, pH = 5.0 ± 0.05, $T = 298$ K, $I = 0.1$ M NaCl

GO colloidal properties at pH = 5.0

To achieve a better understanding of the impact of HA on GO stability in aqueous solution, we investigated the change of nanosheet size distributions before and after solution, GO + U(VI) solution, GO + HA solution, sorption of U(VI) by GO + HA solution (GO + HA + U(VI)), and sorption of HA + U(VI) onto GO solution (HA + U (VI) + GO), were considered at a slightly acidic solution (pH 5.0). The corresponding nanosheet size distributions were shown in Fig. 7, as well as the pictures for each solution (as an inset image in Fig. 7). Except a clear solution C, the other solutions were observed with precipitates, in particularly for solution B, which has the largest amount of precipitates, indicating the largest average nanosheet size.

The size distribution of GO was within 500–2000 nm with an average value of 1036.3 nm (Fig. 7a). The precipitations observed in solution A can be attributed to the homo-aggregation of GO in aqueous solution. The basal plane of GO nanosheets were mainly decorated with hydroxyl and epoxy functional groups and carboxyl groups existed at the edge of the GO sheets [40], which played a key role in determining the solution behavior of GO [41]. According to the Derjaguin–Landau–Verwey–Overbeek (DLVO) theory that both repulsive and attractive potentials existed between GO nanosheets noted as van der Waals (vdW) attraction and electrostatic (EL) repulsion, respectively. With pH decreasing, the protonation of the oxygenated groups of GO gives rise to significant impairment in σ and strength of EL repulsion [42]. Therefore, it is possible for vdW to overcome the repulsive forces if the solution pH is low enough (for example 5.0 in this study), leading to the aggregation of the particles. In a word, the dispersity and aggregation of GO nanosheets depend on the relative intensity of the two opposite interactions by changing pH values. Similar phenomenon was observed and reported by Lei and Tan et al. [21, 43].

The decreased average size from 1036.3 nm (GO solution) to 416.2 nm (GO + HA) after reacting with HA (Fig. 7c) is attributed to the stabilization function of HA to GO nanosheets. HA is amphoteric with both hydrophilic and hydrophobic parts [19]. By mixing HA with GO, the aromatic HA moieties can be adsorbed to GO through π–π interaction and/or hydrophobic interaction [44] and the formation of GO + HA complexes would increase the hydrophilicity of GO + HA complexes by exposing both hydrophilic parts to water. Moreover, the adsorbed HA also acted as a shield to prevent the approaching of GO nanosheets, thus reducing the aggregation of GO nanosheets. Similar behaviors were also reported by mixing PAA (PAA: poly(acrylic acid)) with GO [34] and surfactants with MWCNT [21]. Decreased zeta potential was also observed after mixing HA with GO solutions [29], indicating increased electrostatic repulsion between GO nanosheets. As a result, the average particle size of HA + GO complexes decreased dramatically as compared with pure GO nanosheets.

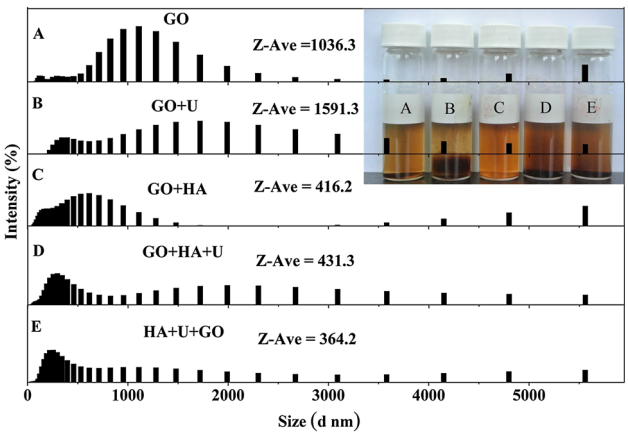

Fig. 7 Particle size of different GO systems, $C_{HA} = 100$ mg L^{-1}, $C_U = 60$ mg L^{-1}, $C_{GO} = 0.133$ g L^{-1}, pH = 5 ± 0.05, reacting time = 1 h

On the contrary, the average size of GO + U increased to 1591.3 nm (Fig. 7b), and the size distribution ranged from 200 to 5000 nm. The sorption of U(VI) onto GO surfaces was believed to proceed via electrostatic attractions between U(VI) and GO surfaces. According to Wang et al. [10], U(VI) sorption is mainly attributed to the strong surface complexation at pH > pH_{pzc} and the aggregation of GO nanosheets is aggravated at high ionic strength. U(VI), when co-exists with GO, can form complexes with GO and it can enhance ionic strength as well, both of which would increase the particle size distributions of GO + U(VI).

A slightly smaller average size distribution was observed for the simultaneous system (HA + U(VI) + GO, Fig. 7e) than the sequential systems (GO + HA + U(VI), Fig. 7d), indicating a slightly better sorption capacity of the simultaneous system, which is consistent with the sorption results in Fig. 6.

Conclusion

In this paper, the influence of HA toward U(VI) sorption onto GO surface were systematically studied. The sorption process is pH dependent and ionic strength independent. The U(VI) sorption capacity can be promoted by the presence of HA and higher HA concentrations resulted in higher sorption capacities. The effect of pre-mixing order was also investigated, indicating a preferred pre-mixing of HA + U(VI) over GO + HA for the U(VI) sorption capacity. The increased sorption capacity can be explained by the average size distributions of different GO systems in aqueous solutions. HA can exfoliate and stabilize GO in aqueous solution by observing smaller average sizes of GO + HA than GO and GO + U(VI). The relative smaller HA + U(VI) + GO than GO + HA + U(VI) further corroborated the better sorption capacity of HA + U(VI) + GO.

Acknowledgments Financial supports from National Science Foundation of China (21272236) and the special scientific research fund of public welfare profession of China (201509074).

References

1. Li L, Xu M, Chubik M, Chubik M, Gromov A, Wei G, Han W (2015) Entrapment of radioactive uranium from wastewater by using fungus-Fe_3O_4 bio-nanocomposites. RSC Adv 5:41611–41616

2. Li ZJ, Wang L, Yuan LY, Xiao CL, Mei L, Zheng LR, Zhang J, Yang JH, Zhao YL, Zhu ZT, Chai ZF, Shi WQ (2015) Efficient removal of uranium from aqueous solution by zero-valent iron nanoparticle and its graphene composite. J Hazard Mater 290:26–33
3. Shi WQ, Yuan LY, Li ZJ, Lan JH, Zhao YL, Chai ZF (2012) Nanomaterials and nanotechnologies in nuclear energy chemistry. Radiochim Acta 100:727–736
4. Zhao Y, Li J, Zhao L, Zhang S, Huang Y, Wu X, Wang X (2014) Synthesis of amidoxime-functionalized Fe_3O_4@SiO_2 core-shell magnetic microspheres for highly efficient sorption of U(VI). Chem Eng J 235:275–283
5. Dabrowski A, Hubicki Z, Podkoscielny P, Robens E (2004) Selective removal of the heavy metal ions from waters and industrial wastewaters by ion-exchange method. Chemosphere 56:91–106
6. Zhao Y, Li J, Zhang S, Chen H, Shao D (2013) Efficient enrichment of uranium(vi) on amidoximated magnetite/graphene oxide composites. RSC Adv 3:18952–18959
7. Buszewski B, Szultka M (2012) Past, present, and future of solid phase extraction: a review. Crit Rev Anal Chem 42:198–213
8. Yang SB, Chen CL, Chen Y, Li JX, Wang DQ, Wang XK, Hu WP (2015) Competitive adsorption of Pb-II, Ni-II, and Sr-II ions on graphene oxides: a combined experimental and theoretical study. Chem Plus Chem 80:480–484
9. Gopalakrishnan A, Krishnan R, Thangavel S, Venugopal G, Kim SJ (2015) Removal of heavy metal ions from pharma–effluents using graphene-oxide nanosorbents and study of their adsorption kinetics. J Ind Eng Chem 30:14–19
10. Wang XX, Chen ZS, Wang XK (2015) Graphene oxides for simultaneous highly efficient removal of trace level radionuclides from aqueous solutions. Sci China Chem 58:1766–1773
11. Sitko R, Turek E, Zawisza B, Malicka E, Talik E, Heimann J, Gagor A, Feist B, Wrzalik R (2013) Adsorption of divalent metal ions from aqueous solutions using graphene oxide. Dalton Trans 42(16):5682–5689
12. Romanchuk AY, Slesarev AS, Kalmykov SN, Kosynkin DV, Tour JM (2013) Graphene oxide for effective radionuclide removal. Phys Chem Chem Phys: PCCP 15(7):2321–2327
13. Xie Y, Helvenston EM, Shuller-Nickles LC, Powell BA (2016) Surface Complexation Modeling of Eu(III) and U(VI) Interactions with Graphene Oxide. Environ Sci Technol 50(4):1821–1827
14. Liu Y, Zhang D, Pang S, Liu Y, Shang Y (2015) Size separation of graphene oxide using preparative free-flow electrophoresis. J Sep Sci 38(1):157–163
15. MacCarthy P, Suffet IH (1989) Aquatic humic substances and their influence on the fate and treatment of pollutants. ACS Symp Ser 219:R17–R30
16. Gaffney JS, Marley NA, Clark SB (1996) In humic and fulvic acids: isolation, structure, and environmental role. In: ACS symposium series, vol 651. American Chemical Society, Washington, DC, pp 2–16
17. Ghosh K, Schnitzer M (1980) Macromolecular structures of humic substances. Soil Sci 129:266–276
18. Santamara-Fernndez R, Cave MR, Hill SJ (2003) The effect of humic acids on the sequential extraction of metals in soils and sediments using ICP-AES and chemometric analysis. J Environ Monit 5:929–934
19. Steelink C (1963) What is humic acid? J Chem Educ 40:379–384
20. Han Z, Zhang F, Lin D, Xing B (2008) Clay minerals affect the stability of surfactant-facilitated carbon nanotube suspensions. Environ Sci Technol 42:6869–6875
21. Tan X, Fang M, Chen C, Yu S, Wang X (2008) Counterion effects of nickel and sodium dodecylbenzene sulfonate adsorption to multiwalled carbon nanotubes in aqueous solution. Carbon 46:1741–1750
22. William S, Hummers J, Offeman Richard E (1958) Preparation of graphitic oxide. J Am Chem Soc 80:1339
23. Stankovich S, Dikin DA, Piner RD, Kohlhaas KA, Kleinhammes A, Jia Y, Wu Y, Nguyen ST, Ruoff RS (2007) Synthesis of graphene-based nanosheets via chemical reduction of exfoliated graphite oxide. Carbon 45:1558–1565
24. Schniepp HC, Li JL, McAllister MJ, Sai H, Herrera-Alonso M, Adamson DH, Prud'homme RK, Car R, Saville DA, Aksay IA (2006) Functionalized single graphene sheets derived from splitting graphite oxide. J Phys Chem B 110:8535–8539
25. Xu YX, Bai H, Lu GW, Li C, Shi GQ (2008) Flexible graphene films via the filtration of water-soluble noncovalent functionalized graphene sheets. J Am Chem Soc 130:5856–5857
26. Mohanty N, Moore D, Xu Z, Sreeprasad TS, Nagaraja A, Rodriguez AA, Berry V (2012) Nanotomy-based production of transferable and dispersible graphene nanostructures of controlled shape and size. Nat Commun 3:844
27. Zhang W, Zou X, Li H, Hou J, Zhao J, Lan J, Feng B, Liu S (2015) Size fractionation of graphene oxide sheets by the polar solvent-selective natural deposition method. RSC Adv 5(1):146–152
28. Wang X, Bai H, Shi G (2011) Size fractionation of graphene oxide sheets by pH-assisted selective sedimentation. J Am Chem Soc 133(16):6338–6342
29. Chen YM, Ren CX, Ouyang SH, Hu XG, Zhou QX (2015) Mitigation in multiple effects of graphene oxide toxicity in zebrafish embryogenesis driven by humic acid. Environ Sci Technol 49:10147–10154
30. Parkhurst DL, Appelo C (1999) User's guide to PHREEQC (Version 2)—a computer program for speciation, batch-reaction, one dimensional transport, and inverse geochemical calculations, U.S. Geological Survey Water-Resources Investigations Report
31. Shih CJ, Lin SC, Sharma R, Strano MS, Blankschtein D (2012) Understanding the pH-dependent behavior of graphene oxide aqueous solutions: a comparative experimental and molecular dynamics simulation study. Langmuir 28:235–241
32. Yuan LY, Liu YL, Shi WQ (2011) High performance of phosphonate-functionalized mesoporous silica for U(VI) sorption from aqueous solution. Dalton Trans 40:7446–7453
33. Shao DD, Li JX, Tan XL, Yang ZS, Okuno K, Oya Y (2015) XPS investigation of impurities containing boron films affected by energetic deuterium implantation and thermal desorption. J Nucl Mater 457:118–123
34. Ren XM, Li JX, Tan XL, Shi WQ, Chen CL, Shao DD, Wang XK (2014) Impact of Al_2O_3 on the aggregation and deposition of graphene oxide. Environ Sci Technol 48:5493–5500
35. Sun YB, Shao DD, Chen CL, Yang SB, Wang XK (2013) Highly efficient enrichment of radionuclides on graphene oxide supported polyaniline. Environ Sci Technol 47:9904–9910
36. Chen YQ, Chen LB, Bai H, Li L (2013) Graphene oxide–chitosan composite hydrogels as broad-spectrum adsorbents for water purification. J Mater Chem A 1:1992–2001
37. Lai CH, Chen CY, Wei BL, Yeh SH (2002) Cadmium adsorption on goethite-coated sand in the presence of humic acid. Water Res 36:4943–4950
38. Yang S, Li LY, Pei ZG, Li CM, Shan XQ, Wen B, Zhang SZ, Zheng LR, Zhang J, Xie YN, Huang RX (2014) Effects of humic acid on copper adsorption onto few-layer reduced graphene oxide and few-layer graphene oxide. Carbon 75:227–235
39. Song WC, Shao DD, Lu SS, Wang XK (2014) Simultaneous removal of uranium and humic acid by cyclodextrin modified graphene oxide nanosheets. Sci China Chem 57:1291–1299
40. Dreyer DR, Park S, Bielawski CW, Ruoff RS (2010) The chemistry of graphene oxide. Chem Soc Rev 39:228–240
41. Li XL, Zhang GY, Bai XD, Sun XM, Wang XR, Wang E, Dai HJ (2008) Highly conducting graphene sheets and Langmuir-Blodgett films. Nat Nanotechnol 3:538–542

42. Gudarzi MM (2016) Colloidal stability of graphene oxide: aggregation in two dimensions. Langmuir 32:5058–5068
43. Wu L, Liu L, Gao B, Munoz-Carpena R, Zhang M, Chen H, Zhou ZH, Wang H (2013) Aggregation kinetics of graphene oxides in aqueous solutions: experiments, mechanisms, and modeling. Langmuir 29:15174–15181
44. Lee BM, Seo YS, Hur J (2015) Investigation of adsorptive fractionation of humic acid on graphene oxide using fluorescence EEM-PARAFAC. Water Res 73:242–251